2014 IEEE International Conference on Robotics & Automation (ICRA)
Hong Kong Convention and Exhibition Center
May 31 - June 7, 2014. Hong Kong, China

Study of Limit Cycle in Antagonistically Coupled Magneto-Rheological Actuators

Peyman Yadmellat and Mehrdad R. Kermani

***Abstract*— In this paper, the presence of limit cycles in the behavior of antagonistically coupled Magneto-Rheological (MR) actuators is investigated. The actuator considered in this paper was developed and described in [1] and [2]. This actuator offers high torque-to-mass and torque-to-inertia ratios, for inherent safe actuation. While the antagonistic arrangement is beneficial in improving the actuator performance and eliminating backlash, it may result in limit cycles when the actuator operates in a position control loop. The occurrence of limit cycle depends on the parameters of the actuator as well as the controller. An in-depth analysis is carried out in this paper to establish a connection between the system parameters and the limit cycle occurrence. Moreover, sufficient conditions for avoiding limit cycle are derived specifically for a Proportional-Derivative (PD) controller. Simulations and experimental results validate the analysis and provide insights into the limit cycle observed in the operation of antagonistic MR actuators.**

I. Introduction

Limit cycles are self-excited oscillations in nonlinear systems, the characteristics of which are irrespective to initial conditions. Such a periodic solution emerges as a closed trajectory in the phase portrait of a nonlinear system. In particular, the limit cycle oscillation is an undesirable response to positioning control systems that can cause mechanical failure. As experimentally observed, antagonistic actuation based on Magneto-Rheological (MR) fluids can give rise to limit cycles in position control loops. This paper aims at establishing the dependency of limit cycle occurrence on the parameters of MR actuators.

MR fluids are non-homogenous suspensions of micrometer-sized ferromagnetic particles in a carrier fluid. The apparent viscosity of MR fluids can be adjusted by an external magnetic field. The suspended particles in the fluid form columns (chains) aligned to the direction of the applied field that results in shearing or flow resistance in the fluid. The degree of the resistive force is related to the strength of the magnetic field, resulting in a field dependent yield stress in MR fluids [3], [4]. In the absence of a magnetic field, MR fluids act as Newtonian fluids whose viscosity change proportional to the shear rate.

Controllability and fast response of MR fluids to external magnetic field have made them an attractive technology for a broad range of applications from civil engineering to automotive, robotics, and rehabilitation applications (e.g. see [5]–[7]). Particularly, in robotics, MR actuators can be employed in series with active drives (e.g. motors) to control the delivery of the output torque at the joints. Benefits of a controllable actuator utilizing MR fluids have been recognized in various robotic applications including haptic devices [8]–[10] and human-robot interaction [2], [11]–[13].

As the main contribution of this paper, a careful and in-depth analysis of the occurrence of limit cycles in the operation of an antagonistic MR actuator is performed. To this end, the dynamic model of the antagonistic actuator is formulated. Considering the system in a feedback loop, a set of simulations is carried out to provide insights to the occurrence of the limit cycle in the actuator response. The describing function method [14, Ch. 7] is then employed to predict the possibility of limit cycle oscillation in the actuator response. The frequency and amplitude of the oscillations are analytically derived and their dependencies on the system parameters and PD controller are studied. Sufficient conditions under which limit cycle oscillations can be prevented are obtained. The results are experimentally validated using a planar robot utilizing MR actuators as a test bench.

The rest of this paper is organized as follow: Section II introduces antagonist actuators based on MR fluids along with discussion on MR fluids characteristics. A nonlinear model of an antagonistic MR actuator is also derived in this section. Section III presents the main contribution of this paper, where the occurrence of limit cycles is analyzed, and the amplitude and frequency of the resultant limit cycle is obtained. In Section IV, simulation and experimental results are provided to validate our theoretical analysis. Finally, Section V concludes the paper.

II. Magneto-Rheological Fluid-Based Actuation

The torque-velocity behavior of an MR actuator is formulated in this section. Fig. 1 depicts the Distributed Active-Semi Active (DASA) actuation concept. In this arrangement, the active drive provides power to the joint, via an MR clutch that controls the output torque. A drawback of DASA actuation is the need for the motor velocity to revers for bi-directional actuation, resulting in backlash in geared actuation. Moreover, the performance of the actuation will be limited by the performance of the active drive. To address the problem, the DASA actuation can be extended to an antagonistic configuration [2].

Antagonistic actuation provides bi-directional actuation by utilizing a single unidirectional motor (see Fig. 2). In this configuration, two MR clutches receive rotational motion in opposite direction from a motor that provides a unidirectional

This work was supported in part by the Natural Sciences and Engineering Research Council (NSERC) of Canada under Grant RGPIN 346166 and Ontario of Centres of Excellence (OCE) under Grant MR 90545.

The authors are with the Electrical and Computer Engineering Department, the University of Western Ontario, London, ON N6A 5B9 Canada pyadmell@uwo.ca, mkermani@eng.uwo.ca.

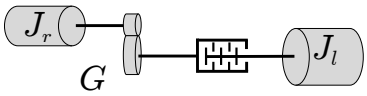

Fig. 1. DASA Configuration. G is the gear ratio. J_r and J_l represent rotor and link's inertias, respectively.

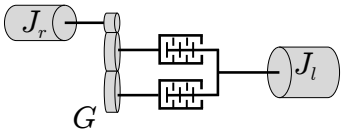

Fig. 2. Antagonistic DASA Configuration. G is the gear ratio. J_r and J_l represent rotor and link's inertias, respectively.

rotation. This can be simply achieved using differential gearing. In this way, the net torque delivered to the joint in both direction can be changed without altering the motor direction. While eliminating backlash in the gears and/or transmission belts. This is due to the fact that neither gears nor the transmission belts lose their engagements with the motor.

In general, the behavior of MR actuators depends on the MR fluid characteristics and the geometry of the actuator. The effects of the MR fluids and geometrical parameters of the actuator on the operation of A-DASA actuation are explained in the following subsections.

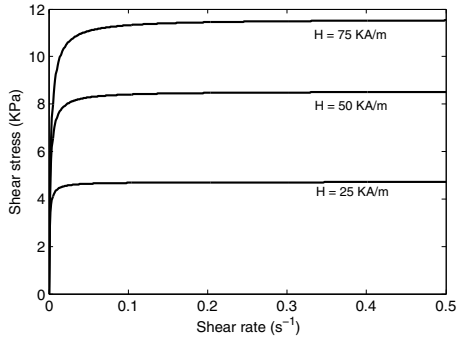

Fig. 3. Shear stress vs. shear rate in a sample MR fluid.

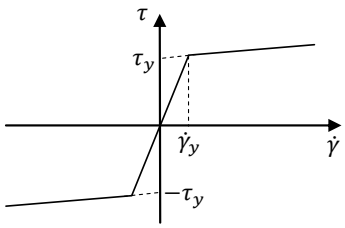

Fig. 4. Biviscous model of MR fluids.

A. Models for MR Fluids

Fig. 3 shows the shear stress-shear rate behavior of a sample MR fluid, which qualitatively represents the typical behavior of MR fluids [15]. As observed, the behavior of an MR fluid can be divided into two main phases; pre-yielding and post-yielding regions. The behavior of MR fluids varies from viscoelastic in the pre-yielding region to plastic in the post-yielding, and it is visco-plastic in the transition through yielding. This type of behavior suggests a biviscous characteristic (see Fig. 4), where the fluid behavior

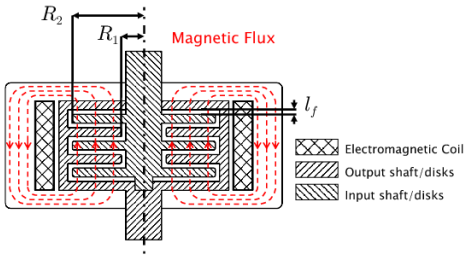

Fig. 5. Cross-section of a multi-disk MR clutch.

switches between pre- and post-yielding behaviours, as can be expressed by,

$$\tau = \begin{cases} \tau_y(H)\text{sgn}(\dot{\gamma}) + \eta\dot{\gamma}, & |\dot{\gamma}| \geq \dot{\gamma}_y \\ \eta_r\dot{\gamma}, & |\dot{\gamma}| < \dot{\gamma}_y \end{cases} \tag{1}$$

where η_r is the elastic property of the fluid, and $\dot{\gamma}_y$ has the following relationship with the yield stress,

$$\dot{\gamma}_y = \tau_y(H)/\left(\eta_r - \eta\right). \tag{2}$$

B. A-DASA Model

Fig. 5 shows the cross–section of a typical multi–disk MR clutch. The input shaft breaks out into a set of input disks which are aligned in parallel to a set of output disks attached to the output shaft. MR fluid fills the volume between input and output disks. By energizing the electromagnetic coil, the shear stress of MR fluids, thereby the output torque of the clutch can be controlled. Considering this arrangement, the shear rate of MR fluids at radius ρ equals to

$$\dot{\gamma}(\rho) = \dot{\theta}_r\rho l_f^{-1}, \tag{3}$$

where $\dot{\theta}_r$ is the angular velocity between the input and output shafts, and l_f is the gap between the input and output disks. The torque produced by a circumferential element at a radius ρ is given by,

$$dT = 2\pi\rho^2\tau d\rho, \tag{4}$$

where τ is the shear stress as defined in (1). Assuming that the clutches in antagonistic configuration are identical, and each clutch has N output disks, the torque transmitted through either of the clutches can be obtained after substituting (1) into (4) and integrating across both faces of each output disk. After some algebraic manipulations, one can obtain,

$$T_i = \begin{cases} \wp_1\tau_y(H_i)\text{sgn}(\dot{\theta}_{r_i}) + \wp_2\dot{\theta}_{r_i}, & |\dot{\theta}_{r_i}| \geq \dot{\theta}_y \\ \wp_3\tau_y(H_i)\text{sgn}(\dot{\theta}_{r_i}) + \wp_4\dot{\theta}_{r_i} & \textit{O.W.}, \end{cases} \tag{5}$$

where $T_i, i \in \{1,2\}$ is the output torque of the i-th clutch, $H_i, i \in \{1,2\}$ is the applied magnetic field to the corresponding clutch, $\dot{\theta}_{r_1} = (\dot{\theta}_m - \dot{\theta}_l)$ and $\dot{\theta}_{r_2} = (-\dot{\theta}_m - \dot{\theta}_l)$, $\dot{\theta}_m$ and $\dot{\theta}_l$ are, respectively, the input and output shafts velocities, and the coefficients $\wp_i, i \in 1,2,3,4$ are defined as,

$$\begin{aligned} \wp_1 &= 4N\pi(R_2^3 - R_1^3)/3, \\ \wp_2 &= N\pi\eta(R_2^4 - R_1^4)/l_f, \\ \wp_3 &= 4N\pi(R_2^3 - R^3)/3, \\ \wp_4 &= N\pi\left(\eta R_2^4 - \eta_r R_1^4 + R^4(\eta_r - \eta)\right)/l_f, \end{aligned} \tag{6}$$

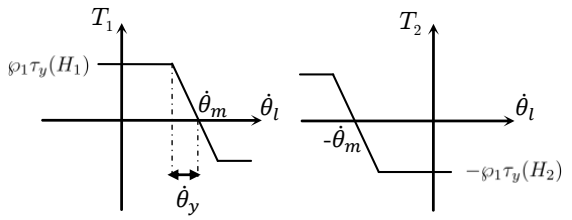

Fig. 6. Torque-velocity relationship of the A-DASA actuator.

where R_1 and R_2 are the inner and outer radii of the disks, respectively, $\dot{\theta}_y = l_f\dot{\gamma}_y R_1^{-1}$, $R = \min\{R_2, l_f\dot{\gamma}_y/|\dot{\theta}_{r_i}|\}$. The total torque of the actuator T equals to the summation of T_1 and T_2, i.e.

$$T(H_1, H_2, \dot{\theta}_l, \dot{\theta}_m) = T_1(H_1, \dot{\theta}_l, \dot{\theta}_m) + T_2(H_2, \dot{\theta}_l, \dot{\theta}_m). \quad (7)$$

Considering (5), the output torque of each clutch in an A-DASA actuator is depicted in Fig. 6, where the effect of the fluid viscosity is neglected, i.e. $\eta \approx 0$. Since $|\dot{\theta}_{r_i}| < \dot{\theta}_y$ corresponds to the pre-yielding phase of MR fluids ($|\dot{\gamma}| < \dot{\gamma}_y$), a roll-off phenomenon occurs in the operation of the actuator for $|\dot{\theta}_{r_i}| < \dot{\theta}_y$, when the output torque of the actuator decreases in absolute value, depending on the value of $\wp_4$. In a typical MR actuator, this phenomenon results in zero acceleration at velocities closed to the motor velocity, as such the output shaft velocity $\dot{\theta}_l$ remains in a bounded region, i.e. $|\dot{\theta}_l| \leq \theta_m$.

In general, the output torque of the actuator can be controlled by adjusting the applied magnetic fields to the clutches and varying the motor velocity. It is however favourable to set the motor velocity to a constant value greater than the maximum desired velocity and control the torque solely by the applied magnetic fields, i.e. H_1 and H_2.

III. Limit Cycle Analysis

The behavior of A-DASA actuation in feedback control loop is studied in this section. This study requires a dynamic model of the controlled system. Fig. 7 shows a position control scheme for the A-DASA actuation, in which $G_c(s)$ and $G_l(s)$ are the transfer functions of the controller and the output shaft mechanical subsystem, respectively. The dynamic equations of the system can be expressed as,

$$\begin{aligned} \dot{H}_1 &= -\lambda_1 H_1 + c_1 S|i(t)|, \\ \dot{H}_2 &= -\lambda_2 H_2 + c_2(1-S)|i(t)|, \\ \ddot{\theta}_l &= -\frac{b}{J}\dot{\theta}_l + \frac{1}{J}T(H_1, H_2, \dot{\theta}_l, \dot{\theta}_m), \end{aligned} \quad (8)$$

where $i(t)$ is the input current commanded by the controller, λ_i and $c_i, i \in \{1, 2\}$ are the magnetic circuit parameters, J is the inertia of the output shaft, b represents the viscous friction coefficient, and the switching variable S is defined as below,

$$S = \begin{cases} 1, & i(t) \geq 0 \\ 0, & i(t) < 0 \end{cases} \quad (9)$$

Since the output torques of the clutches counteract with each other, it is more efficient to power only one clutch at a time.

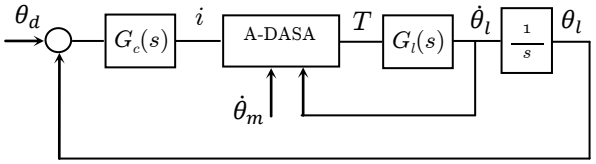

Fig. 7. Position control block diagram using A-DASA actuation.

Note that the yield stress of the MR fluid is independent of the applied magnetic field, hence the applied current.

A. Assumptions and Preliminaries

In order to use describing function method, the system is required to be presented as an interconnection of linear subsystems and a nonlinearity. Referring to Fig. 7, the dynamic model of the A-DASA subsystem is required. Defining the post-yielding torque T_y as follows,

$$T_y = \begin{cases} \wp_1\tau_y(H_1), & i(t) \geq 0 \\ -\wp_1\tau_y(H_2), & i(t) < 0 \end{cases} \quad (10)$$

Linearizing (10) around $H_1 = H_2 = 0$ yields,

$$T_y \simeq \begin{cases} \wp_1\nu H_1, & i(t) \geq 0 \\ -\wp_1\nu H_2, & i(t) < 0 \end{cases} \quad (11)$$

where ν is defined as, $\nu = \frac{\partial\tau_y(H)}{\partial H}\big|_{H=0}$.

Considering (8) and (10), the time derivative of T_y can be obtained as,

$$\begin{aligned} \dot{T}_y &\simeq \begin{cases} \wp_1\nu\dot{H}_1, & i(t) \geq 0 \\ -\wp_1\nu\dot{H}_2, & i(t) < 0 \end{cases} \\ &\simeq \begin{cases} -\lambda_1 T_y + \wp_1\nu c_1 i(t), & i(t) \geq 0 \\ -\lambda_2 T_y + \wp_1\nu c_2 i(t) & i(t) < 0 \end{cases} \end{aligned} \quad (12)$$

Considering that both clutches and their magnetic circuits are identical, and assuming $\lambda_1 = \lambda_2 = \lambda, c_1 = c_2 = c$, we have,

$$\dot{T}_y \simeq -\lambda T_y + c_T i(t), \quad (13)$$

for $c_T = \wp_1\nu c$.

Given the fact that the effect of the fluid viscosity is neglectable[1], the output torque of the A-DASA actuator is approximately equal to T_y when the actuator operates in the post-yielding region. In the event that the actuator enters the pre-yielding region, the output torque will decrease in absolute value reciprocal to the growth of the output shaft velocity due to roll-off (see (5)). The position control block diagram of the system can be represented as shown in Fig. 8, where $G_T(s)$ is the transfer function between the post-yielding torque and the input current, and the nonlinearity $\psi(\dot{\theta}_l)$ imitates the roll-off phenomenon defined as,

$$\psi(\dot{\theta}_l) = \begin{cases} 0, & |\dot{\theta}_l| \leq \dot{\theta}_m - \dot{\theta}_y \\ -\wp_4\dot{\theta}_l, & O.W. \end{cases} \quad (14)$$

[1]The viscosities of MR fluids are typically in the range of 0.1 to 0.3 Pa-s.

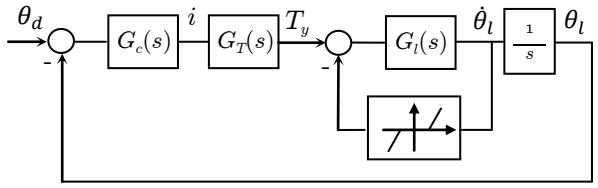

Fig. 8. Equivalent position control block diagram of the A-DASA actuation.

The describing function method can now be used to analysis the possibility of limit cycles. In this method, the system is assumed to be a *free* system; that is, the system is only excited by the initial conditions and the system inputs are zero. The basic idea behind the analysis is to derive conditions under which the system is capable of regenerating a sinusoid, if the input to the nonlinearity is sinusoidal. This condition is met when the closed-loop gain of the system from the nonlinearity input back to the nonlinearity equals to unity. Hence, the system exhibits limit cycle behavior, regenerating the same sinusoidal response.

B. Analysis

To derive the conditions for limit cycle, a function $\Psi(A)$ is defined as,

$$\Psi(A) = \frac{2\omega}{\pi A}\int_0^{\pi\omega} \psi(A\sin\omega t)dt. \tag{15}$$

where $\Psi(A)$ is called the describing function of $\psi(\cdot)$, and can be regarded as an equivalent gain of the nonlinearity when exposed to a sinusoidal input $A\sin(\omega t)$. Introducing (14) into (15), the describing function $\Psi(\omega, A)$ can be obtained as,

$$\Psi(A) = \begin{cases} 0, & A \le \dot{\theta}_m - \dot{\theta}_y \\ -\wp_4\left\{1 - \Psi_s(\frac{A}{\dot{\theta}_m - \dot{\theta}_y})\right\} & A > \dot{\theta}_m - \dot{\theta}_y \end{cases} \tag{16}$$

where

$$\Psi_s(x) = \frac{2}{\pi}\left\{\sin^{-1}\frac{1}{x} + \frac{1}{x}\cos(\sin^{-1}\frac{1}{x})\right\}. \tag{17}$$

According to (8) and (13), $G_l(s)$ and $G_T(s)$ can be described as,

$$G_l(s) = \frac{k_l}{\tau_l s + 1}, G_T(s) = \frac{k_T}{\tau_T s + 1}, \tag{18}$$

where

$$k_l = J^{-1}, \tau_l = Jb^{-1}, k_T = c_T\lambda^{-1}, \tau_T = \lambda_T^{-1}. \tag{19}$$

Considering $G_c(s)$ as a PD controller, the closed-loop transfer function of the system can then be expressed as,

$$G(j\omega) = \frac{-\left(k_p + jk_d\omega\right)G_T(j\omega)G_l(j\omega)}{j\omega(1 + \Psi(A)G_l(j\omega))}. \tag{20}$$

Introducing (18) into (20), one can obtain,

$$\begin{aligned} G(j\omega) &= \frac{-\left(k_p + jk_d\omega\right)k_T k_l}{j\omega(j\omega\tau_l + k_l\Psi(A) + 1)(j\omega\tau_T + 1)} \\ &= \frac{-\left(k_p + jk_d\omega\right)k_T k_l}{-\alpha\omega^2 + j\omega\left(\beta - \omega^2\tau_l\tau_T\right)} \\ &= \frac{k_T k_l\left(k_p + jk_d\omega\right)\left(\alpha\omega^2 + j\omega\left(\beta - \omega^2\tau_l\tau_T\right)\right)}{\alpha^2\omega^4 + \omega^2\left(\beta - \omega^2\tau_l\tau_T\right)^2}. \end{aligned} \tag{21}$$

where $\alpha = \tau_l + \tau_T\beta$ and $\beta = 1 + k_l\Psi(A)$. A limit cycle *probably* exists if (21) equals unity. Equating (21) to unity results in the following conditions,

$$\Re\{G(j\omega)\} = 1, \Im\{G(j\omega)\} = 0 \tag{22}$$

where $\Re\{G\}$ and $\Im\{G\}$ are real and imaginary parts of the transfer function $G(j\omega)$, as written below,

$$\begin{aligned} \Re\{G(j\omega)\} &= \frac{k_T k_l\left(\alpha k_p - k_d(\beta - \tau_l\tau_T\omega^2)\right)}{\alpha^2\omega^2 + \left(\beta - \omega^2\tau_l\tau_T\right)^2} \\ \Im\{G(j\omega)\} &= \frac{k_T k_l\left(k_p\beta - \omega^2(k_p\tau_l\tau_T - k_d\alpha)\right)}{\alpha^2\omega^3 + \omega\left(\beta - \omega^2\tau_l\tau_T\right)^2}. \end{aligned} \tag{23}$$

Considering the condition on the imaginary part in (22) yields the frequency of the limit cycle as follows,

$$\begin{aligned} \omega &= \sqrt{\frac{k_p\beta}{k_p\tau_l\tau_T - k_d\alpha}} \\ &= \sqrt{\frac{k_p(1 + k_l\Psi(A))}{k_p\tau_l\tau_T - k_d(\tau_l + \tau_T + \tau_T k_l\Psi(A))}}. \end{aligned} \tag{24}$$

Furthermore, substituting ω in (23) and applying the condition on the real part in (22) results in the following condition, after some algebraic manipulations,

$$p_4\beta^4 + p_3\beta^3 + p_2\beta^2 + p_1\beta + p_0 = 0, \tag{25}$$

where

$$\begin{aligned} p_0 &= k_T k_l k_p\tau_l^3(k_p\tau_T - k_d)^2, \\ p_1 &= \tau_l^2(k_p\tau_T - kd)(k_T k_l\tau_T^2 k_p^2 - k_p\tau_l + k_T k_l k_d^2 \\ &\quad -3k_p k_T k_l\tau_T k_d), \\ p_2 &= \tau_l(k_d - k_p\tau_T)(2k_p\tau_l\tau_T + 2k_p k_T k_l\tau_T^2 k_d - k_d\tau_l \\ &\quad -2k_T k_l k_d^2\tau_T), \\ p_3 &= \tau_T(k_p\tau_T - k_d)(k_T k_l k_d^2\tau_T + 2k_d\tau_l - k_p\tau_l\tau_T), \\ p_4 &= \tau_T^2 k_d(k_p\tau_T - k_d), \end{aligned}$$

By solving (25) for β, four solutions re obtained of which two of them are always negative, one is always positive, and one can be positive depending on the parameters of the system. Since $\beta \ge 0$ by definition, two acceptable solutions are,

$$\beta = \begin{cases} k_p\tau_l/k_d \\ \frac{\sqrt{\tau_l^2 - 2\tau_l k_T k_l\tau_T k_d + k_T^2 k_l^2\tau_T^2 k_d^2 + 4k_T k_l\tau_T^2\tau_l k_p}}{2\tau_T} \\ \quad -\frac{\tau_l + k_T k_l\tau_T k_d}{2\tau_T}. \end{cases} \tag{26}$$

Subsequently, $\Psi(A)$ can be calculated as,

$$\Psi(A) = \frac{\beta - 1}{k_l}. \tag{27}$$

A limit cycle is predicted for any non-zero positive A that satisfies the equality given in (27). This is equivalent to the transfer function of the closed-loop system to be unity for the specified A and ω. Consequently, an oscillation will be regenerated in the loop, resulting in a limit cycle behavior.

C. Discussion

Recalling (22), no ω can be found to satisfy the condition on the imaginary part of $G(j\omega)$ given in (23), if,

$$k_d \geq \frac{k_p \tau_l \tau_T}{\alpha} = \frac{k_p \tau_l \tau_T}{\tau_l + \tau_T \beta}. \quad (28)$$

That is, no limit cycle can be occurred for any k_d satisfying (28). Since the minimum value of β equals to one, no limit cycle presents if

$$k_p \leq \frac{k_d(\tau_l + \tau_T)}{\tau_l \tau_T}. \quad (29)$$

Therefore, at least one of the system time constants should be designed to be as small as possible in order to increase the allowable bound for k_p. The value of τ_l depends on the output shaft inertia and the inertia of the robot link attached to the actuator. Decreasing τ_l corresponds to reducing the robot link inertia, which may not be feasible. It is therefore required to minimize τ_T, which is a function of the actuator geometry alone[2]. In conclusion, high bandwidth magnetic circuit is essential if the goal is to avoid the occurrence of limit cycles and attain high performance.

IV. Experimental Validations and Simulation

In this section, a set of model-based simulations along with experimental results are provided to validate our analysis. The experimental results were carried out using a 2-DOF manipulator. The 2-DOF manipulator (see Fig. 9) utilizes MR clutches as part of its actuation system. Two MR clutches configured antagonistically are used to actuate the first joint, while the second joint is actuated using a single MR clutch and a spring (for more details on the design of the manipulator see [12]). The antagonistic joint was only used in this set of experiments. The specifications of the MR clutches used in this manipulator were given in Table I. The robot link inertia is 0.13 kg.m^2. The manipulator is driven by a brushless motor (BLWRPG235D-36V-4000-R13) to provide the rotational inputs to the MR clutches. The motor is driven by a driver in the velocity control mode. The manipulator incorporates two encoders (HEDS-9000) to measure the angular positions of the joints. Three high-power motor drivers (AMC-AZ12A8), set in current mode, provide the command currents to the MR clutches. In our experiments, both controllers were implemented on a desktop computer connected to the manipulator via a dSPACE (DS 1103) controller board. The sampling frequency for gathering experimental data was set to 1 kHz.

A. Model-based Simulations

The A-DASA actuation in Fig.7 for position control was considered. The output torque of the actuator was modeled by (5) and (7). The response of the system was simulated by solving the ordinary differential equation (8) in Matlab,

[2] τ_T depends on the magnetic field time constant. The magnetic field time constant is a function of the coil inductance and the reluctance of the magnetic circuit forming magnetic flux. Both parameters depend on the internal dimensions of the actuator, and can be optimised in the actuator design stage.

TABLE I
Specifications of the A-DASA system

MR fluid type	MRF-140CG
MR fluid gap thickness (l_f)	0.5 mm
No. of input disks (N)	2
Inner radius of the disks (R_1)	44.9 mm
Outer radius of the disks (R_2)	50.4 mm
λ_1, λ_2	7.69
Coil constant ($c_1 = c_2$)	0.5 Km^{-1}
Moment of inertia (J)	3.7×10^{-3} Kg.m^2
Viscous friction coefficient (b)	0.4×10^{-3} Kg.m^2.s

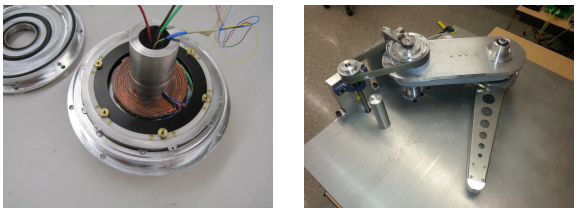

Fig. 9. A snap shot of the MR clutch during fabrication and the 2-DOF MR-actuator robot manipulator.

considering the inertia of the robot link. Fig. 10 shows the simulation results for $k_p = 0.1$ and $k_d = 0$. As observed, no limit cycle was occurred. Fig. 11 shows the results for $k_p = 0.5$ and $k_d = 0$ when a limit cycle occurs in the response. Based on the previous analysis, adding k_d can eliminate the limit cycle if the value of k_d is chosen to be greater than $\underline{k}_d$. The calculated value of $\underline{k}_d$ for the current system is $\underline{k}_d = 0.025$. To validate the results, the response of the system was simulated using two different values for k_d. Fig. 12 compares the results for $k_d = 0.01$ ($k_d < \underline{k}_d$) and $k_d = 0.026$. The results clearly show that limit cycle oscillations can be avoided by applying $k_d \geq \underline{k}_d$. On the other hand for $k_d < \underline{k}_d$, the response of the system is trapped in a limit cycle. Increasing the derivative gain further in this case will alleviate the problem and allow the response to converge to the origin. This validates the results derived in this paper.

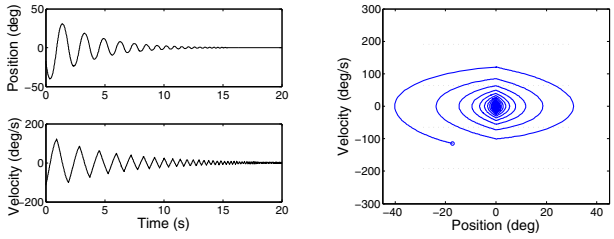

(a) (b)

Fig. 10. (a) Simulated angular position and velocity of the 1st joint, (b) Phase portrait of the A-DASA in position control; $k_p = 0.1$, $k_d = 0$. The initial condition is marked by a circle.

B. Preliminary Experiments

The occurrence of limit cycle was investigated using the 2-DOF robot. Fig. 13 shows the experimental results for two different proportional gains. The proportional gains were $k_p = 1$ and $k_p = 2$, respectively. To perturb the robot from

its steady state, a 100 mA current was applied at $t = 2s$ and removed at $t = 4s$. As seen, the frequency of the response changes with respect to the controller gain. Referring to (24), it can be shown that the limit cycle frequency for a P controller (for $k_d = 0$) can be approximated by,

$$\omega \simeq \sqrt{\frac{k_p k_T k_l}{\tau_l}}. \tag{30}$$

According to (30), the frequency of the limit cycle is expected to grow proportionally with the root square of k_p. The limit cycle frequencies for $k_p = 1$ and $k_p = 2$ were $f = 1.9048$ Hz and $f = 2.4876$ Hz, respectively. The limit cycle frequency for $k_p = 2$ is approximately $\sqrt{2}$ times the frequency of $k_p = 1$, confirming the theoretical analysis.

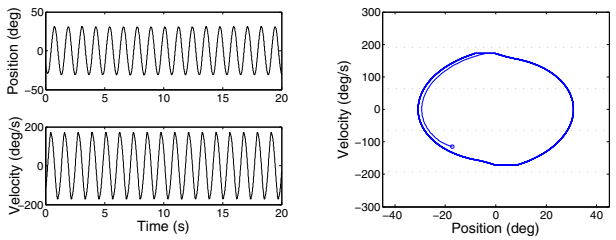

(a) (b)

Fig. 11. (a) Simulated angular position and velocity of the 1st joint,(b) Phase portrait of the A-DASA in position control; $k_p = 0.5$, $k_d = 0$. The initial condition is marked by a circle.

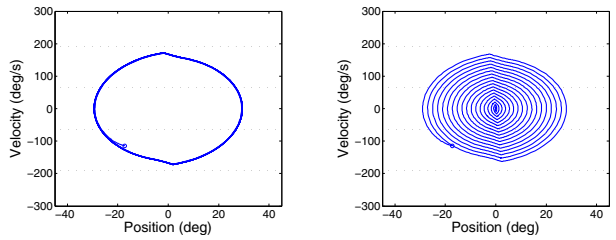

(a) (b)

Fig. 12. Phase portrait of the A-DASA in position control; (a) $k_p = 0.5$, $k_d = 0.01$, (b) $k_p = 0.5$, $k_d = 0.026$. The initial condition is marked by a circle.

V. Conclusion

In this paper, the occurrence of limit cycles in the behavior of an antagonistically coupled MR actuators was discussed. A practical example was studied to demonstrate the possibility of limit cycle induced by the antagonistic arrangement of the actuators when operated in the position control loop. Using describing function method, the dependency of the limit cycle on the actuator parameters was thoroughly analyzed, and the results were demonstrated. Further, the frequency and amplitude of the resultant limit cycle were analytically derived as functions of the system parameters. It was shown that the limit cycle oscillations could be prevented for specific PD controller gains. As an important observation, it was discussed that high-bandwidth magnetic circuits were essential in eliminating the limit cycle. Numerical simulations along with experimental results validated the theoretical analysis. The insight gained in this paper can be used as a foundation for the design of antagonistically coupled MR actuators as well as the design of controllers aiming at the limit cycle prevention.

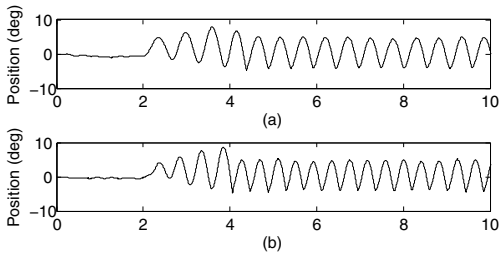

Fig. 13. Experimental results using the 2-DOF robot; (a) $k_p = 1$, (b) $k_p = 2$.

References

[1] A. S. Shafer and M. R. Kermani, "On the feasibility and suitability of MR fluid clutches in human-friendly manipulators," *Mechatronics, IEEE/ASME Transactions on*, no. 99, pp. 1–10, 2011.

[2] P. Yadmellat, A. S. Shafer, and M. R. Kermani, "Development of a safe robot manipulator using a new actuation concept," in *Robotics and Automation (ICRA), 2013 IEEE International Conference on*. IEEE, 2013, pp. 337–342.

[3] K. D. Weiss, T. G. Duclos, J. D. Carlson, M. J. Chrzan, and A. Margida, *High strength magneto-and electro-rheological fluids*. Society of Automotive Engineers, 1993.

[4] M. R. Jolly, J. W. Bender, and J. D. Carlson, "Properties and applications of commercial magnetorheological fluids," *Journal of Intelligent Material Systems and Structures*, vol. 10, no. 1, pp. 5–13, 1999.

[5] O. Ashour, C. A. Rogers, and W. Kordonsky, "Magnetorheological fluids: Materials, characterization, and devices," *Journal of Intelligent Material Systems and Structures*, vol. 7, no. 2, pp. 123–130, March 1996.

[6] D. J. Peel, R. Stanway, and W. A. Bullough, "Experimental study of an er long-stroke vibration damper," in *Smart Structures and Materials 1997: Passive Damping and Isolation*, L. P. Davis, Ed., vol. 3045, no. 1. SPIE, 1997, pp. 96–107.

[7] J. D. Carlson and D. M. Catanzarite, "Magnetorheological fluid devices and process of controlling force in exercise equipment utilizing same," October 1998.

[8] A. Bicchi, M. Raugi, R. Rizzo, and N. Sgambelluri, "Analysis and design of an electromagnetic system for the characterization of magnetorheological fluids for haptic interfaces," *Magnetics, IEEE Transactions on*, vol. 41, no. 5, pp. 1876–1879, 2005.

[9] F. Ahmadkhanlou, G. N. Washington, Y. Wang, and S. E. Bechtel, "The development of variably compliant haptic systems using magnetorheological fluids," in *12th SPIE International Symposium, San Diego, CA*, 2005.

[10] B. Liu, W. Li, P. Kosasih, and X. Zhang, "Development of an MR-brake-based haptic device," *Smart materials and structures*, vol. 15, no. 6, p. 1960, 2006.

[11] T. Saito and H. Ikeda, "Development of normally closed type of magnetorheological clutch and its application to safe torque control system of human-collaborative robot," *Journal of Intelligent Material Systems and Structures*, vol. 18, no. 12, pp. 1181–1185, 2007.

[12] P. Yadmellat, A. Shafer, and M. Kermani, "Design and development of a single-motor, two-dof, safe manipulator," *Mechatronics, IEEE/ASME Transactions on*, in press, doi:10.1109/TMECH.2013.2281598.

[13] T. Kikuchi, K. Otsuki, J. Furusho, H. Abe, J. Noma, M. Naito, and N. Lauzier, "Development of a compact magnetorheological fluid clutch for human-friendly actuator," *Advanced Robotics*, vol. 24, no. 10, pp. 1489–1502, 2010.

[14] H. K. Khalil, *Nonlinear systems*. Prentice hall Upper Saddle River, 2002, vol. 3.

[15] F. Ahmadkhanlou, M. Mahboob, S. Bechtel, and G. Washington, "An improved model for magnetorheological fluid-based actuators and sensors," *Journal of Intelligent Material Systems and Structures*, vol. 21, no. 1, pp. 3–18, 2010.